The Journal of Immunology

Lymphatic Specific Disruption in the Fine Structure of Heparan Sulfate Inhibits Dendritic Cell Traffic and Functional T Cell Responses in the Lymph Node

Xin Yin, Scott C. Johns, Daniel Kim, Zbigniew Mikulski, Catherina L. Salanga, Tracy M. Handel, Mónica Macal, Elina I. Zúñiga and Mark M. Fuster

J Immunol 2014; 192:2133-2142; Prepublished online 3 February 2014;
doi: 10.4049/jimmunol.1301286
http://www.jimmunol.org/content/192/5/2133

The Journal of Immunology is published twice each month by
The American Association of Immunologists, Inc.,
1451 Rockville Pike, Suite 650, Rockville, MD 20852

Print ISSN: 0022-1767 Online ISSN: 1550-6606.

Lymphatic Specific Disruption in the Fine Structure of Heparan Sulfate Inhibits Dendritic Cell Traffic and Functional T Cell Responses in the Lymph Node

Xin Yin,*[,†,‡] Scott C. Johns,[†,‡] Daniel Kim,[†,§] Zbigniew Mikulski,[¶] Catherina L. Salanga,[‖] Tracy M. Handel,[‖] Mónica Macal,[#] Elina I. Zúñiga,[#] and Mark M. Fuster[†,‡]

Dendritic cells (DCs) are potent APCs essential for initiating adaptive immunity. Following pathogen exposure, trafficking of DCs to lymph nodes (LNs) through afferent lymphatic vessels constitutes a crucial step in the execution of their functions. The mechanisms regulating this process are poorly understood, although the involvement of certain chemokines in this process has recently been reported. In this study, we demonstrate that genetically altering the fine structure (*N*-sulfation) of heparan sulfate (HS) specifically in mouse lymphatic endothelium significantly reduces DC trafficking to regional LNs in vivo. Moreover, this alteration had the unique functional consequence of reducing $CD8^+$ T cell proliferative responses in draining LNs in an ovalbumin immunization model. Mechanistic studies suggested that lymphatic endothelial HS regulates multiple steps during DC trafficking, including optimal presentation of chemokines on the surface of DCs, thus acting as a co-receptor that may function "in *trans*" to mediate chemokine receptor binding. This study not only identifies novel glycan-mediated mechanisms that regulate lymphatic DC trafficking, but it also validates the fine structure of lymphatic vascular-specific HS as a novel molecular target for strategies aiming to modulate DC behavior and/or alter pathologic T cell responses in lymph nodes. *The Journal of Immunology*, **2014, 192: 2133–2142.**

Dendritic cells (DCs) are the most potent APCs, and their usual roles center on initiating both protective immunity as well as immunological tolerance. Upon exposure to Ags, DCs exhibit superior capacity to take up and process Ags, undergo maturation, migrate to draining lymph nodes (LNs), and present Ags to naive T cells. The trafficking of DCs from the periphery to the LNs via afferent lymphatic vessels represents a critical element for the execution of DC functions. The overall process has multiple steps, including local chemotaxis through extracellular matrix, adhesion to lymphatic endothelium, transendothelial migration, intralumen transit following lymph flow, and adhesion to, as well as extravasation from, lymphatic vessels in LNs. Trafficking of DCs to the LN depends on many chemokine/receptor interactions, among which the CCR7-CCL21/CCL19 axis appears to be the most potent and best characterized. The LN-homing chemokine receptor CCR7 is upregulated upon DC maturation. Through interactions with its cognate ligands CCL19 and CCL21, which are produced by LN stromal cells and lymphatic endothelial cells (LECs), CCR7 facilitates directional migration of Ag-presenting DCs toward regional LNs (1, 2). Besides CCR7-CCL21/CCL19 crosstalk, other receptor/chemokine complexes, such as CXCR4/CXCL12, are also implicated in regulating DC migration to LNs (3). Despite the biological significance of chemokines, the mechanistic importance of macromolecules that simultaneously control the actions of multiple chemokines along the intervening lymphatic conduit remains poorly understood. However, complex carbohydrates (glycans) bound on cell surface as well as matrix proteoglycans are thought to be important regulators.

Heparan sulfate (HS) is a negatively charged, linear polysaccharide that regulates many cellular processes, including proliferation, adhesion, migration, endocytosis, and signal transduction. The glycan achieves this regulation through interactions with a variety of protein ligands, including growth factors such as basic fibroblast growth factor, various species of vascular endothelial growth factors, chemokines such as IL-8, CCL21, and CXCL12, and possibly others (4). Recent studies in our laboratory demonstrate that lymphatic endothelial HS modulates the optimal presentation of chemokine CCL21 both in *cis* (on $CCR7^+$ lymphatic endothelium) and in *trans* (on $CCR7^+$ migrating cells), thereby cooperating with the formation of chemokine gradients to ultimately facilitate chemokine receptor–mediated migration signaling (5). As a functional consequence of this regulation, disrupting the biosynthesis of lymphatic endothelial HS by targeting either HS

*Marine Drug Research Institute, Huaihai Institute of Technology, Lianyungang 222005, China; [†]Veterans Affairs San Diego Healthcare System, Medical and Research Services, San Diego, CA 92161; [‡]Division of Pulmonary and Critical Care, Department of Medicine, University of California San Diego, La Jolla, CA 92037; [§]School of Medicine, University of California San Diego, La Jolla, CA 92037; [¶]La Jolla Institute for Allergy and Immunology, La Jolla, CA 92037; [‖]Skaggs School of Pharmacy and Pharmaceutical Sciences, Department of Pharmacology, University of California San Diego, La Jolla, CA 92037; and [#]Division of Biological Sciences, University of California San Diego, La Jolla, CA 92037

Received for publication May 14, 2013. Accepted for publication December 25, 2013.

This work was supported by National Institutes of Health/National Heart, Lung, and Blood Institute Grant R01-HL107652-01A1 (to M.M.F.), with additional support from Grant P01 HL57345-14; National Institutes of Health/National Institute of Allergy and Infectious Diseases Grant R01-AI37113 (to T.M.H.); National Institute of General Medical Sciences Ruth L. Kirschstein Minority Access to Research Centers Predoctoral Fellowship funding (to C.L.S.); and by National Institutes of Health/National Heart, Lung, and Blood Institute Training Grant T32HL098062 (to X.Y.). This work was also supported by National Institutes of Health/National Institute of Allergy and Infectious Diseases Grants R01-081923 and R21-AI102247 (to E.I.Z.), as well as by U.S. Department of Veterans Affairs Merit Award I01BX000987-01 (to M.M.F.) and by American Cancer Society Grant RSG-08-153-01-CSM (to M.M.F.).

Address correspondence and reprint requests to Dr. Mark M. Fuster, Veterans Affairs San Diego Healthcare System and University of California San Diego, Department of Medicine, Division of Pulmonary and Critical Care, 3350 La Jolla Village Drive, San Diego, CA 92161. E-mail address: mfuster@ucsd.edu

The online version of this article contains supplemental material.

Abbreviations used in this article: BMDC, bone marrow–derived dendritic cell; CM, conditioned medium; DC, dendritic cell; hLEC, human lymphatic endothelial cell; HS, heparan sulfate; LEC, lymphatic endothelial cell; LN, lymph node; Ndst1, *N*-deacetylase/*N*-sulfotransferase-1; PLA, proximity ligation assay; siDS, control small interfering RNA; siRNA, small interfering RNA.

www.jimmunol.org/cgi/doi/10.4049/jimmunol.1301286

chain initiation or chain sulfation significantly reduces chemokine-dependent trafficking of tumor cells in the lymphatic system (5). So far, however, our understanding of how lymphatic traffic by DCs is modulated in the lymphatic microenvironment, including mechanisms that control multiple chemokines, remains very limited. For CCL21 in particular, work in our laboratory, as well as a study examining the effects of a global vascular disruption of HS chain elongation on multiple forms of cell traffic to the LN, showed that altering HS chains on the lymphatic endothelial cell surface impaired adhesion between CCL21 and lymphatic endothelium (5, 6). Additionally, gradients of CCL21 in the perilymphatic space have been shown to be altered following chemical disruption of HS in the extracellular matrix (7, 8). These observations raise questions as to what a lymphatic vascular-specific genetic disruption in the fine structure of HS might do not only to DC traffic, but also to the ultimate T cell responses in the LN upstream from an antigenic stimulus.

In this study, we hypothesized that disruption of lymphatic HS will inhibit the trafficking of Ag-loaded DCs to regional LNs as well as Ag-dependent T cell activation. We also hypothesized that specific fine structural modifications of lymphatic HS (which can be genetically targeted) may uniquely affect DC trafficking. To test our hypothesis, we examined the significance of genetically altering the sulfation of lymphatic endothelial HS on the trafficking of DCs to regional LNs, and we explored underlying mechanisms. We also assessed the subsequent effects on T cell immunity. Our results reveal novel glycan-specific modifications and mechanisms that regulate lymphatic DC traffic, and they validate the fine structure of lymphatic HS as a potential molecular target for therapeutic approaches to modulate DC behavior and/or correct pathologic immune responses.

Materials and Methods

Cell culture and treatments

Primary human lung LECs (hLECs; Lonza, Basel, Switzerland) were cultured in EBM2 endothelial basal medium supplemented with an EGM2 bullet kit (Lonza). Bone marrow–derived dendritic cells (BMDCs) were isolated from the femurs and tibias of C57BL/6 mice (8–12 wk of age) and differentiated with GM-CSF (20 ng/ml; PeproTech, Rocky Hill, NJ) as previously described (9). Unless otherwise stated, BMDCs at day 9 of differentiation were used for experiments. All small interfering RNA (siRNA) duplexes were from Integrated DNA Technologies (Coralville, IA) and were transfected into cells according to the manufacturer's instructions. For heparinase treatment, cells were incubated with heparinase (heparin lyases I, II, and III; 2.5 mU/ml; provided by Dr. Jeffrey D. Esko, University of California San Diego) in serum-free EBM2 medium at 37˚C, 5% CO_2 for 1 h. To block specific chemokine or chemokine receptor signaling, cells were incubated with Abs against CCL21 (1:100), CXCL12 (1:50), CCL5 (1:100), CXCR4 (1:100), or CCR7 (1:100; R&D Systems, Minneapolis, MN) at 37˚C, 5% CO_2 for 1 h (for adhesion and transmigration assays under shear flow), 6 h (for transwell migration assays), or overnight (for transwell invasion assays).

Animals

All animal experiments were reviewed and approved by the Institutional Animal Care and Use Committee of the University of California San Diego. Mice between 4 and 8 wk of age were used in this study. Lymphatic-specific *N*-deacetylase/*N*-sulfotransferase-1 (Ndst1) mutants (designated $Ndst1^{f/f}Prox1^{+/CreERT2}$) and their wild-type littermates ($Ndst1^{f/f}Prox1^{-/CreERT2}$) were generated by breeding tamoxifen-inducible $Prox1^{+/CreERT2}$ transgenic mice (kindly provided by Dr. G. Oliver at St. Jude Children's Research Hospital, Memphis, TN) extensively backcrossed onto the C57BL/6 background with $Ndst1^{f/f}$ conditional mutant mice. To induce the activity of Cre recombinase, tamoxifen (Sigma-Aldrich, St. Louis, MO) dissolved in corn oil was i.p. injected into the mice at 0.12 mg/g body weight daily for 5 consecutive days. In separate pilot studies, mice were found to tolerate this schedule well, remained with stable body weight, and behaved normally following tamoxifen injections. All mice were maintained in a pathogen-free facility on a 12-h light/dark cycle with food and water provided ad libitum.

Skin painting

FITC (6.6 mg/ml; Sigma-Aldrich) and oxazolone (30 mg/ml; Sigma-Aldrich) were dissolved in 95% ethanol and painted onto the shaved abdomen of mice (200 μl/mouse). After 40 h, inguinal and axillary lymph nodes were isolated and digested with 0.2% type I collagenase at 37˚C for 1 h. Digested samples were filtered through a 40-μm cell strainer and then stained with PE-labeled anti-mouse CD11c Ab (eBioscience, San Diego, CA), and PE/FITC double-positive cells were analyzed by FACSCalibur (BD Biosciences, San Jose, CA).

Whole-mount immunofluorescence staining of mouse ear

Unstimulated tamoxifen-induced mutant versus wild-type mice were sacrificed, and their ears were dissected and separated into dorsal and ventral sheets. The sheets were fixed in 1% paraformaldehyde, permeabilized with PBS containing 0.3% Triton X-100 (PT buffer), blocked with PT buffer supplemented with 3% goat serum, and then incubated with rabbit anti-Lyve1 Ab (1:800; Abcam, Cambridge, MA) overnight at 4˚C. After three washes in 1% BSA/PT buffer, Cy3-conjugated anti-rabbit secondary Ab (Jackson ImmunoResearch Laboratories, West Grove, PA) was added and incubated at room temperature for 2 h. At least five random images were acquired from each sample using the fluorescence microscope, and the $Lyve1^+$ lymphatic vascular area per image was quantified using National Institutes of Health ImageJ software.

Quantification of skin DCs

Skin tissues were mechanically chopped into small pieces and digested in DMEM medium containing 0.8% trypsin and 20 μg/ml DNase I (Sigma-Aldrich) at 37˚C for 1 h on a rocking plate. Digested cells were filtered through a 40-μm cell strainer (BD Biosciences), stained with FITC-labeled anti-mouse CD11c Ab as well as PE-labeled anti-mouse MHC class II Ab (eBioscience), and FITC/PE double-positive cells were analyzed on a FACSCalibur.

Trafficking of in situ–implanted BMDCs

BMDCs at day 9 of differentiation in culture were labeled with calcein AM (eBioscience) and injected into the left foot dorsum of $Ndst1^{f/f}Prox1^{+/CreERT2}$ mutants and their $Ndst1^{f/f}Prox1^{-/CreERT2}$ wild-type littermates (2×10^6 cells/mouse). After 40 h, the left popliteal LN was isolated, imaged under the fluorescence microscope, and digested with 0.2% type I collagenase into a single-cell suspension. Cells from each LN digest were resuspended into 100 μl PBS with 1.5 μl spotted onto the well of a Terasaki microtiter plate (Robbins Scientific, Sunnyvale, CA) and imaged under the fluorescence microscope. The number of $calcein^+$ cells was quantified using National Institutes of Health ImageJ software.

In vivo T cell proliferation in draining LNs

OVA (Sigma-Aldrich) was dissolved into PBS at 5 mg/ml and mixed thoroughly with IFA (Sigma-Aldrich; v/v = 1:1) until a uniform oil-in-water emulsion was formed. The emulsion was then injected i.p. into the mice (200 μl/mouse). Seven days later, 40 μl freshly prepared OVA/IFA emulsion was injected intradermally into the footpad. Five days later, the mice were sacrificed, with popliteal and inguinal LNs from the injected side isolated, digested into single-cell suspensions, stained with Alexa Fluor 488–labeled anti-CD3 together with allophycocyanin-labeled anti-CD4 or allophycocyanin-labeled anti-CD8 Abs (eBioscience) and analyzed by FACSCalibur.

Adoptive transfer of CFSE-labeled T cells and their proliferation in vivo

CD8 T cells were purified from spleens of OT-I mice and CD4 T cells from spleens of OT-II mice (both OT-I and OT-II mice were kindly provided by Dr. Stephen Hedrick, University of California San Diego Division of Biological Sciences) using corresponding Dynabeads Untouched cell isolation kits (Invitrogen, Carlsbad, CA). The purified T cells were labeled with CFSE following an established protocol (10), and a mixture of equal numbers of CFSE-labeled CD4 and CD8 cells (3×10^6/mouse) were adoptively transferred into the mice via retro-orbital injection as previously described (11). After 24 h, the mice were injected with a mixture of the OT-I and OT-II respective peptides, $OVA_{257–264}$ and $OVA_{323–339}$ (1 mg/ml in normal saline and mixed thoroughly with IFA at v/v = 1:1) into the footpad (40 μl/footpad). After 72 h, mice were sacrificed and the popliteal LN on the injected side was isolated and digested into a single-cell suspension using 0.2% type I collagenase at 37˚C for 1 h followed by filtration through a 40-μm cell strainer. Cells were then stained with allophycocyanin-labeled anti-CD4 or allophycocyanin-labeled anti-CD8 Abs (eBioscience) and analyzed by FACSCalibur.

BMDC interactions with hLECs under flow

The hLECs were seeded onto microfluidic channels of BioFlux plates (48-well, 0–20 dynes/cm^2; Fluxion Biosciences, San Francisco, CA) precoated

with Matrigel (1:50 in PBS; BD Biosciences). At ~90% confluence, hLECs were either treated with heparinase, blocking Abs, or transfected with siRNA. For adhesion assays, BMDCs prelabeled with calcein AM following the manufacturer's instruction were perfused into the channel at a concentration of 2×10^6 cells/ml in EBM2 medium under an initial shear stress of 2 dynes/cm^2 for 2 min followed by a constant flow at 0.14 dynes/cm^2 for 15 min. After removing the residual BMDCs from the inlet well, the channel was washed with EBM2 medium at 1 dyne/cm^2 for 5 min to remove any unattached BMDCs. Adherent BMDCs across the whole channel were imaged using a PerkinElmer UltraVIEW VoX spinning disk confocal microscope (×100; University of California San Diego Light Microscopy Facility) and quantified with Metamorph software (Molecular Devices, Sunnyvale, CA). Following the capture of adhesion images at time 0 (t_0), transmigration of adherent BMDCs (defined by disappearance of adherent cells visibly from the surface of the hLEC monolayer to the space beneath the monolayer, as opposed to detachment and carriage out of the viewing field under flow) was observed under a constant shear of 0.14 dyne/cm^2 of cell-free EBM2 medium for another 30 min using the same microscope, with the end point image taken at that time (t_{30}). The percentage transmigration was calculated as [(no. adherent BMDCs at t_0 − no. adherent BMDCs at t_{30})/no. adherent BMDCs at t_0] × 100%.

Transwell invasion and chemotaxis migration assays

To assess the mobility of BMDCs toward hLECs in vitro, a modified transwell invasion and chemotaxis assay was performed as previously described (5). For collagen matrix-based invasion assays, 1×10^5 hLECs were embedded into 100 μl type I collagen gel containing 3 mg/ml PureCol (Advanced Biomatrix, San Diego, CA) in DMEM (pH 7.3), applied to cover the lower side of a transwell insert (3.0 μm in pore size; Corning), and allowed to solidify in a 37°C, 5% CO_2 incubator for 6 h. The insert was then inverted and placed into a 24-well plate containing prewarmed serum-free EBM2 (500 μl/well). For chemotaxis assays, 5×10^4 hLECs/well were seeded directly into the bottom of a 24-well plate and treated. For both assays, 2–5 × 10^5 BMDCs prelabeled with calcein AM were resuspended in 100 μl EBM2 and loaded on top of the insert. For the invasion assay, the plates were placed in a 37°C, 5% CO_2 incubator overnight, and for 6 h in the case of the chemotaxis assays. At the end of the invasion/chemotaxis period, transwells were transferred to a new 24-well plate and treated with either 0.2% type I collagenase (Sigma-Aldrich) for 1 h (for collagen matrix-based invasion assay) or trypsin (Invitrogen, Grand Island, NY) for 5 min (for chemotaxis assay) with gentle rocking at 37°C. Bottom-well solutions were collected, transferred to clean Eppendorf tubes, and centrifuged at 500 × *g* for 5 min. Cell pellets were resuspended in 20 μl PBS with 1.5 μl aliquots loaded onto a 96-well Terasaki plate, and images were taken at ×40 magnification with a Nikon Eclipse 80i fluorescence microscope and analyzed with National Institutes of Health ImageJ software. All experiments were set up in triplicate with at least three independent experiments performed.

Reverse transcription followed by quantitative real-time PCR

Total RNA was extracted from cells using an RNAqueous-4PCR kit (Ambion) and reverse transcribed into cDNA with a SuperScript III kit (Invitrogen) according to the manufacturers' instructions. Real-time PCR was performed with an iQ SYBR Green Supermix kit (Bio-Rad, Hercules, CA). The primer sequences (5′ to 3′) used for real-time PCR were as follows: human Ndst1, forward, GGACATCTGGTCTAAG, reverse, GATGCCTTTGTGATAG; human XylT2, forward, ACGTTCAACCGCAAACTACC, reverse, ATTGCTCAGTTCCCCATCTG; human CCL21, forward, GCCTTGCCACACTCTTTCTC, reverse, CAAGGAAGAGGTGGGGTGTA; and human CCR7, forward, TTCTTCACTGTCCTCCAAGC, reverse, ACATTTCCCTTGTCCTCTCC. The PCR program was as follows: 95°C for 3 min followed by 40 cycles of 95°C for 30 s, 59°C for 30 s, and 72°C for 30 s. Relative expression of target gene against β-actin was calculated using the $2^{-\Delta\Delta Ct}$ method (12).

Preparation of conditioned media from hLECs

To harvest conditioned media (CM), hLECs were transfected with different siRNA molecules, washed once with PBS, and incubated in EBM2/5% horse serum (posttreatment over a DEAE column to clear endogenous sulfated glycosaminoglycans from the serum) for 24 h. The supernatant was then collected and briefly centrifuged to remove the cell debris.

Duolink assay

The specific interactions between chemokines from CM and chemokine receptors on cytospin-collected BMDCs were determined with the Duolink proximity ligation assay (PLA; Olink Bioscience, Uppsala, Sweden) following the manufacturer's instruction using the following primary Abs: anti-CCL21 (R&D Systems, MAB3661, 1:100), anti-CCR7 (Novus, St. Charles, MO; 1:250), anti-CXCL12 (R&D Systems, AF-310-NA, 1:100), and anti-CXCR4 (R&D Systems, MAB172, 1:200).

Purification of HS from hLECs

Purification of HS was performed as previously described (13). Briefly, hLECs in 10-cm tissue culture plates were transfected with different siRNA molecules, washed with PBS once, and digested in 1× Pronase buffer containing 167 μg/ml Pronase (Sigma-Aldrich), 40 mM sodium acetate, and 320 mM sodium chloride in PBS (10 ml buffer/10-cm plate) at 37°C for 24 h. The cellular digest was then filtered through 0.2-μm polyethersulfone syringe filters (GE Healthcare, Piscataway, NJ) and run through a DEAE-Sephacel (GE Healthcare) column by gravity. After washing with DEAE equilibration buffer (0.2 M sodium chloride, 20 mM sodium acetate [pH 6.0]), the glycan components were eluted from the column with DEAE elution buffer containing 2 M sodium chloride and 20 mM sodium acetate (pH 6.0). The salt in the sample was then removed by running the eluent through the PD-10 desalting column (GE Healthcare) following the manufacturer's instruction. The eluted glycans (containing both HS and chondroitin sulfate) were lyophilized, redissolved in chondroitinase buffer (50 mM Tris-HCl [pH 8.0], 50 mM sodium acetate), and digested with chondroitinase A, B, and C (a gift from Dr. Jeffrey Esko, University of California San Diego Department of Cellular and Molecular Medicine) at 37°C for at least 2 h. After another passage through DEAE-Sephacel and PD-10 desalting columns as described above, the purified and lyophilized HS was resupended in PBS (500 μl/10-cm plate).

Oligomerization analysis of CCL21 and CXCL12

Purified PBS-resuspended HS (0.1 μL and 0.3 μL) was incubated separately with recombinant human CCL21 or CXCL12 (20 ng/reaction; PeproTech) in a total reaction volume of 30 μl at room temperature for 1 h followed by crosslinking using BS^3 (Thermo Scientific, Rockford, IL). After quenching the crosslinking reaction with 50 mM Tris, nonreducing protein loading buffer (5× concentration) (Thermo Scientific) was added to the samples, which were then boiled for 5 min and separated on 4–20% gradient gels (Bio-Rad). Samples were then electrotransferred from the gel onto a nitrocellulose membrane and probed with anti-CCL21 or anti-CXCL12 Ab (R&D Systems; 1:1000) followed by IRDye 800 secondary Ab (LI-COR, Lincoln, NE). The signal was detected using the Odyssey infrared imaging system (LI-COR).

Statistical analysis

Quantitative data are presented as means ± SD for three replicates or three independent experiments where indicated. Significance between groups was calculated using a two-tailed Student *t* test. Differences in LN colonization of skin DCs following FITC plus oxazalone painting and that from in situ–implanted BMDCs between mutant and littermate control mice were examined using the rank order test. A p value <0.05 was considered statistically significant.

Results

Tissue-specific inhibition in the sulfation of lymphatic HS impairs in vivo DC trafficking

To test the degree to which the sulfation of HS on lymphatic endothelium plays a role in regulating DC trafficking in vivo, we inducibly and selectively knocked down the gene *Ndst1* in LECs. The Ndst family of enzymes is involved in *N*-sulfation of glucosamine residues during the biosynthesis of nascent HS chains on proteoglycan core proteins (14). The LEC-specific knockdown of *Ndst1* was achieved by crossing mice bearing both loxP-floxed alleles of *Ndst1* (*Ndst1*$^{f/f}$ mice) (13) with mice harboring a tamoxifen-inducible *Cre* allele driven by the lymphatic endothelial specific *Prox1* promoter (*Prox1*$^{+/CreERT2}$ transgenic mice) (5). Previous work has shown that in *Ndst1*$^{f/f}$*Prox1*$^{+/CreERT2}$ mutant mice, five consecutive i.p. injections of tamoxifen potently and selectively reduced *Ndst1* expression in lymphatic endothelial cells, as compared to that of *Ndst1*$^{f/f}$*Prox1*$^{-/CreERT2}$ wild-type control mice (5). After topical application of a solution containing skin allergen oxazolone together with the FITC, FITC$^+$ DCs from the skin to the draining LNs were quantified by flow cytometric staining of FITC$^+$CD11c$^+$ cells. As shown in Fig. 1A, targeting the sulfation of lymphatic endothelial

HS in Cre$^+$ mutant mice significantly reduced the number of FITC$^+$ CD11c$^+$ cells that colonized the draining LN, as compared to that in the Cre$^-$ controls. To examine whether a reduction in lymphatic endothelial *Ndst1* expression in pre-existing unstimulated lymphatic vasculature might lead to any alterations in skin lymphatic vascular density or basal numbers of DCs within skin, we determined the density of Lyve1$^+$ lymphatic vessels in the ear by whole-mount staining, and quantified CD11c$^+$MHC class II$^+$ cells in skin by flow cytometry. As shown in Fig. 1B and 1C, at baseline, there were no significant differences in either lymphatic vascular density or total DC quantity within the skin, suggesting that the reduction in the biosynthesis of lymphatic endothelial HS in pre-existing unstimulated lymphatic vasculature does not alter the conduit by which DCs travel or the basal peripheral pool of DCs prior to Ag uptake, but rather the trafficking process itself.

Considering that painted FITC may not only be taken up by skin-resident DCs, but also might freely diffuse from the skin, reach the draining LN via afferent lymphatic vessels, and be taken up by LN-resident DCs, we also examined in vivo DC trafficking by implanting mutant versus wild-type mice with equal numbers of fluorescence-labeled BMDCs into the foot dorsum, and we quantified DCs that trafficked to the draining LNs by fluorescence microscopy. To achieve this, we followed a well-established protocol for DC differentiation (15) and obtained ~80% marrow-derived CD11c$^+$ DCs after 9-day culture in the presence of GM-CSF (Supplemental Fig. 1A). Further characterization showed that close to 99% of CD11c$^+$ BMDCs were also positive for CD11b but negative for B220 (Supplemental Fig. 1B), consistent with the myeloid immunophenotype of these BMDCs. Fig. 1D shows that by 40 h after in situ DC injection, a significantly lower number of BMDCs travel to the popliteal LN in Cre$^+$ mutant mice as compared to that in *Cre*$^-$ littermate controls.

Genetic targeting of the N*-sulfation of lymphatic endothelial-specific HS inhibits in vivo DC-dependent CD8$^+$ T cell proliferation upon OVA challenge*

To test the biological significance of targeting lymphatic endothelial HS on DC trafficking–dependent T cell responses, we sensitized the mice with an initial dose of the classical Ag OVA. Following a reapplication of OVA into the footpad, we examined the populations of distinct T cell subtypes within the draining LN (Fig. 2A). Using initially a model characterized by a pan-endothelial mutation in *Ndst1*, we found that CD8$^+$ T cell populations were significantly lower in *Ndst1$^{f/f}$TekCre*$^+$ mutant mice than in *Ndst1$^{f/f}$TekCre*$^-$ control littermates (Fig. 2B). Upon restricting the mutation to solely the lymphatic endothelium in vivo (using an inducible *Prox1Cre* transgenic model to drive lymphatic-specific disruption in *Ndst1* expression), a similar reduction in CD8$^+$ T cell proliferation in response to immunization was also observed in *Ndst1*$^{f/f}$*Prox1*$^{+/CreERT2}$ mutants as compared to that in *Ndst1*$^{f/f}$ *Prox1*$^{-/CreERT2}$ littermate controls (Fig. 2C). In this model, when compared to vehicle (IFA)-injected mice, we observed a significant

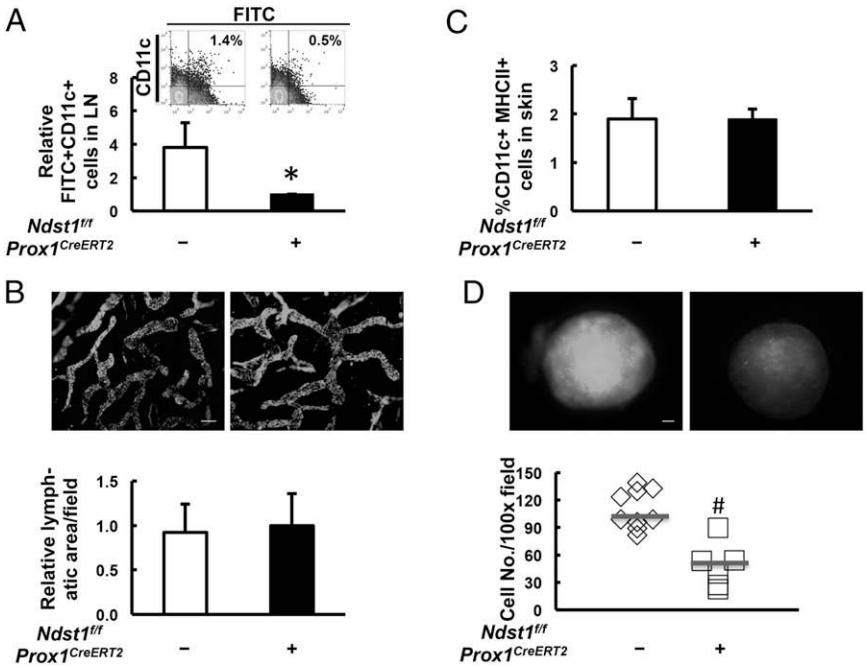

FIGURE 1. Lymphatic endothelial-specific mutation impairing the sulfation of HS inhibits in vivo trafficking of DCs. (**A**) *Ndst1*$^{f/f}$*Prox1*$^{+/CreERT2}$ mutant mice (n = 11) and their *Ndst1*$^{f/f}$*Prox1*$^{-/CreERT2}$ littermates (n = 12) were painted with FITC plus oxazolone on the abdomen. After 40 h, the draining inguinal and axillary LNs were isolated and digested into a single-cell suspension. Percentages of FITC$^+$CD11c$^+$ cells within LNs were analyzed by flow cytometry and averaged following normalization to the mean value of the *Ndst1*$^{f/f}$*Prox1*$^{+/CreERT2}$ group. Data represent the mean of three independent experiments. A representative example of the flow cytometric data is shown in the *inset*. (**B**) Lymphatic vascular density was determined in unstimulated *Ndst1*$^{f/f}$*Prox1*$^{+/CreERT2}$ mutant mice (n = 4) and in *Ndst1*$^{f/f}$*Prox1*$^{-/CreERT2}$ littermates (n = 5) by immunofluorescence staining of Lyve1 (white/gray signal) on ear whole-mount. Representative images are shown in *upper section* (scale bar, 100 μm), and the averages of Lyve1$^+$ lymphatic area per field are shown in *lower graph*, with the level of lymphatic density in mutant mice arbitrarily defined as 1. (**C**) Percentage of CD11c$^+$MHC class II$^+$ DCs in the skin of *Ndst1*$^{f/f}$ *Prox1*$^{+/CreERT2}$ mutants (n = 7) and *Ndst1*$^{f/f}$*Prox1*$^{-/CreERT2}$ littermate controls was determined by flow cytometry. (**D**) BMDCs at day 9 of differentiation in culture were labeled with calcein AM and injected into the left foot dorsum of *Ndst1*$^{f/f}$*Prox1*$^{+/CreERT2}$ mutants (n = 6) and *Ndst1*$^{f/f}$*Prox1*$^{-/CreERT2}$ littermate controls (n = 9) (2×10^6 cells/mouse). After 40 h, the left popliteal LN was isolated, imaged under the fluorescence microscope (*upper panel*; white/gray signal; scale bar, 200 μm), and digested into a single-cell suspension. Cells from each LN digest were resuspended into 100 μl PBS with 1.5 μl spotted onto the well of a Terasaki microtiter plate and imaged under the fluorescence microscope. The number of calcein$^+$ cells was quantified using National Institutes of Health ImageJ software, plotted, and averaged for each genotype [horizontal bars in (D)]. $^*p < 0.05$, $^\#p < 0.01$, as compared to the *Ndst1*$^{f/f}$*Prox1*$^{-/CreERT2}$ group.

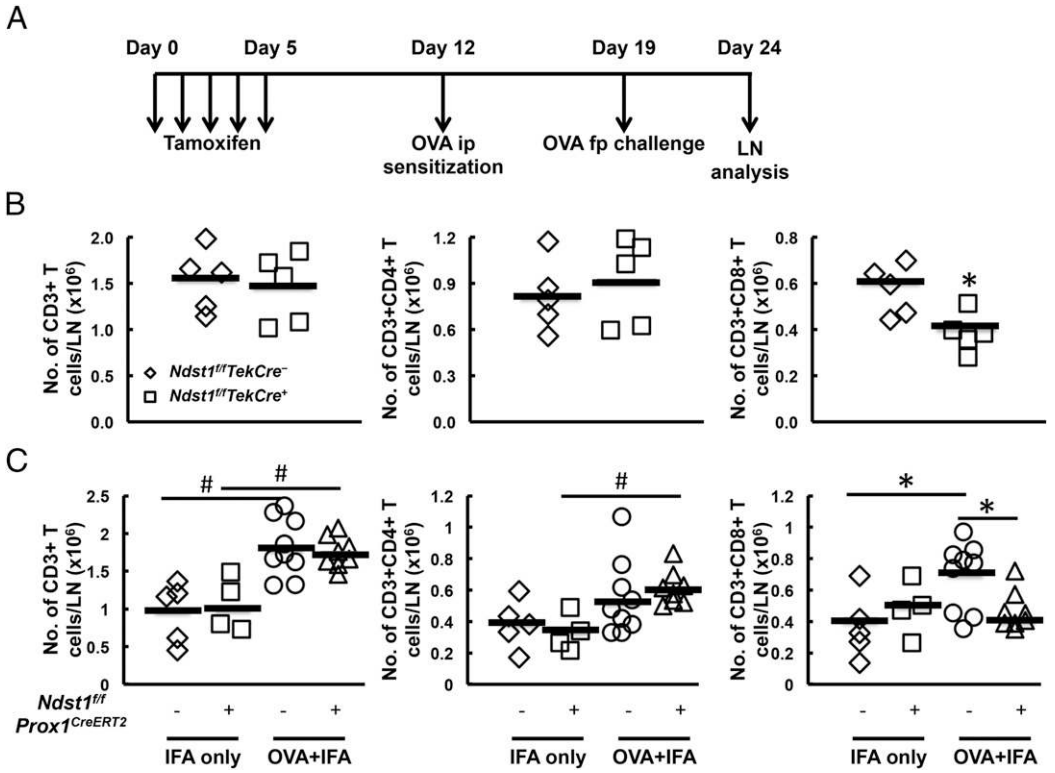

FIGURE 2. Lymphatic endothelial-specific reduction in the *N*-sulfation of HS results in the inhibition of $CD8^+$ T cell proliferation upon OVA challenge. (**A**) Scheme of the experiment. All animals were pretreated with daily tamoxifen for 5 consecutive days to activate *Cre* recombinase. On day 12, a sensitizing dose of OVA (500 μg/mouse) was administered i.p. Seven days later (day 19), 10 μg OVA was delivered to the left footpad by intradermal injection. On day 24, the left popliteal LNs were isolated, with distinct populations of T cells examined by flow cytometry. The experiment was first carried out in animals bearing a panvascular mutation in *Ndst1*. (**B**) Number of $CD3^+$, $CD3^+CD4^+$, and $CD3^+CD8^+$ T cells in the draining LN was compared between $Ndst1^{f/f}TekCre^+$ ($n = 5$) and $Ndst1^{f/f}TekCre^-$ control littermates ($n = 5$). $^*p < 0.05$, as compared to $Ndst1^{f/f}TekCre^-$ control group. (**C**) Number of $CD3^+$, $CD3^+CD4^+$, and $CD3^+CD8^+$ T cells in draining LNs was compared between $Ndst1^{f/f}Prox1^{+/CreERT2}$ mutants ($n = 8$) and $Ndst1^{f/f}Prox1^{-/CreERT2}$ littermates ($n = 9$) after either vehicle control (IFA only) or OVA challenge (OVA plus IFA). $^*p < 0.05$, $^\#p < 0.01$.

increase in the total T cell ($CD3^+$) population upon OVA challenge in both $Ndst1^{f/f}Prox1^{+/CreERT2}$ mutants and $Ndst1^{f/f}Prox1^{-/CreERT2}$ littermates (with only a slight but insignificant reduction in the response of mutants), indicating that T cell proliferation occurred in both groups of animals. Importantly, however, although a significant $CD8^+$ T cell proliferation response occurred in Cre^- wild-type littermates, the $CD8^+$ T cell response was strikingly absent in $Ndst1^{f/f}Prox1^{+/CreERT2}$ mutants. Alternatively, a relatively lesser degree of $CD4^+$ T cell proliferation occurred in both groups (Fig. 2C, *middle panel*), although significance relative to the response in IFA-only controls was only achieved in the mutant group. Thus, the most dramatic effect in this model involving a highly lymphatic-specific deficiency in the *N*-sulfation of HS was the contrast between the $CD8^+$ T cell proliferative response in wild-type mice and the complete lack of such a response in the *Ndst1* mutants (Fig. 2C, *right panel*).

The OVA model employed in Fig. 2 involves two-step stimulation with Ag. To more directly examine how a single immunization on the mutant background might, as a result of altered DC trafficking, affect lymph node T cell proliferation, we adoptively transferred CFSE-labeled OT-I CD8 and OT-II CD4 T cells (expressing transgenic T cell receptors for peptides $OVA_{257–264}$ and $OVA_{323–339}$, respectively) into $Ndst1^{f/f}Prox1^{+/CreERT2}$ versus $Ndst1^{f/f}Prox1^{-/CreERT2}$ mice. At 72 h following footpad injection of a mixture of two specific OVA-derived Ags, namely $OVA_{257–264}$ and $OVA_{323–339}$ peptides, we examined CD8 and CD4 proliferation within the draining popliteal lymph nodes by flow cytometry. As shown in Supplemental Fig. 2, we observed a significant reduction in the ratio of $CFSE^{int}CD8^+$ to $CFSE^{hi}CD8^+$ in $Ndst1^{f/f}Prox1^{+/CreERT2}$ mutant mice as compared to that in $Ndst1^{f/f}Prox1^{-/CreERT2}$ controls. Considering that $CFSE^{int}CD8^+$ cells represented adoptively transferred and actively proliferating CD8 T cells (as compared with nonproliferating $CFSE^{hi}CD8^+$ cells), the ratio of these two populations reflects the proliferative activity of the adoptively transferred CD8 T cells in vivo. Alternatively, no dramatic difference was noted in proliferating $CFSE^+$ CD4 T cells between the two genotypes.

In addition to a phenotype that appears to depend on the trafficking of DCs in distinct lymphatic beds in the two-step model in Fig. 2, secondary effects by cell types other than DCs in the model nevertheless have the potential to influence T cell responses. Accordingly, we characterized the baseline level of distinct cellular components within the peripheral blood (by complete blood count) and the skin-draining lymph nodes (by flow cytometry) from $Ndst1^{f/f}Prox1^{+/CreERT2}$ versus $Ndst1^{f/f}Prox1^{-/CreERT2}$ mice following tamoxifen injection. The two genotypes at baseline showed no significant differences in the complete blood count profile (Supplemental Table 1A), and there were no significant differences in baseline levels of T/B cells, NK cells, and monocytes within the skin-draining LNs (Supplemental Table 1B). We also compared distinct DC subpopulations, including $CD8\alpha^+$ resident DCs, $PDCA1^+$ plasmacytoid DCs, and migratory DCs in the skin-draining LNs of $Ndst1^{f/f}Prox1^{+/CreERT2}$ versus $Ndst1^{f/f}Prox1^{-/CreERT2}$ mice at baseline, and identified no dramatic differences (Supplemental Table 1C).

Altering lymphatic endothelial HS affects DC adhesion but not transmigration under low shear flow

To understand which biological processes during DC trafficking are affected by targeting lymphatic endothelial HS, we first set up an in vitro flow system whereby DCs derived from bone marrow progenitor cells were introduced under low shear flow into a chamber lined with a confluent layer of hLECs. To target hLEC HS in vitro, two general approaches were applied: 1) enzymatic pretreatment of hLECs with heparinase [destroys HS chains (16)], and 2) altering HS biosynthesis (including specific sulfate modifications) in the hLECs through efficient siRNA targeting of specific HS biosynthetic enzymes (Supplemental Fig. 3A). After 15 min under shear flow, a moderate number of DCs were adherent to hLECs, whereas this was dramatically reduced if the hLECs were pretreated with heparinase or blocking Ab to CCR7 (Fig. 3A, *upper panels*, 3B, *upper graph*). Significant reduction in DC adhesion was also observed for hLECs pretreated with CCL21-neutralizing Ab (Fig. 3B, *upper graph*). When hLECs were transfected with siRNA targeting *Ndst1* or *XylT2* (the latter is required for initiating the biosynthesis of glycosaminoglycan chains on core proteins), adhesion was also significantly reduced (Fig. 3B, *lower graph*). However, pretreatment with CCL5-neutralizing Ab or transfection with siRNA targeting Hs3st1 (enzyme responsible for glucoronyl 3-*O*-sulfation of HS) did not alter adhesion. Following DC adhesion under flow, we monitored DC transmigration across the hLEC monolayer. In addition to the effect on adhesion, Abs for CCR7 or CCL21 markedly inhibited DC transmigration (Fig. 3A, *lower panels*, 3C, *upper graph*). In contrast, neither heparinase nor siRNA targeting the different HS biosynthetic enzymes significantly affected DC transmigration (Fig. 3C). These findings imply that CCL21–CCR7 binding and signaling plays an essential role in mediating both DC adhesion to and transmigration across hLEC layers. Alternatively, it appears that HS-mediated adhesion, at least in this model, is not required for transmigration. (Note that the force of gravity in such studies may also potentially contribue to engagement interactions that may be necessary for diapedesis.)

Lymphatic endothelial HS promotes the directional invasion and chemotaxis of DCs

We also assessed the role of lymphatic endothelial HS in modulating DC invasion/chemotaxis transwell-based systems in vitro. To mimic the in vivo physiological step by which DCs invade into extracellular matrix surrounding LECs, we designed a modified in vitro collagen matrix-based transwell assay (5) where hLECs were embedded in type I collagen on the underside of transwell

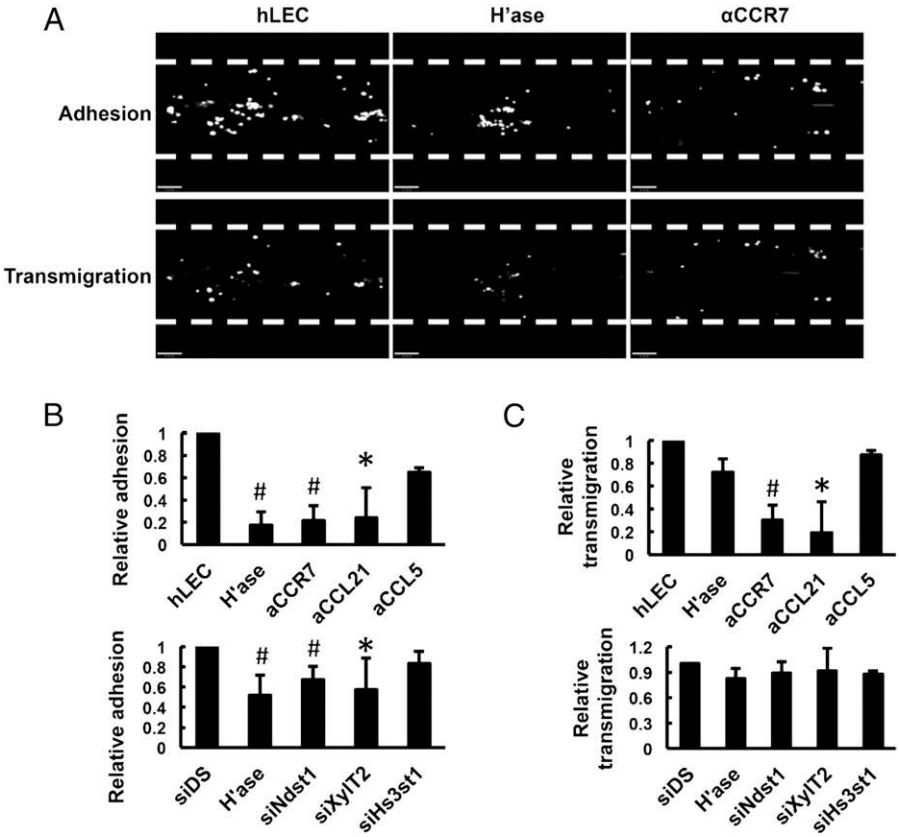

FIGURE 3. Lymphatic endothelial HS critically regulates chemokine-dependent adhesion of BMDCs under low-level physiologic shear flow. hLECs were seeded into a BioFlux flow chamber (edges marked by dashed lines) and pretreated with neutralizing Abs (against CCL21, CCR7, or CCL5) or siRNA targeting the indicated HS biosynthetic enzymes (siDS). Day 9 BMDCs were labeled with calcein AM and introduced into the chamber at a constant shear stress of 0.14 dyne/cm^2 at 37°C. After 15 min, nonadherent cells were washed off and the adherent BMDCs were imaged using fluorescence microscopy [(**A**) *upper panels*, fluorescence in white/gray over black flow channel background], quantified with Metamorph software, and normalized to hLEC control group [*upper graph* in (**B**)] and to the siDS control group for siRNA-targeting experiments [*lower graph* in (**B**)]. The transmigration of adherent BMDCs was recorded following an additional 30-min cell-free flow period (from t_0 to t_{30}), imaged under a fluorescence microscope [*lower panels* in (A)] and quantified using Metamorph software, with the percentage transmigration calculated as [(no. adherent BMDCs at t_0 − no. adherent BMDCs at t_{30})/no. adherent BMDCs at t_0] × 100%. All transmigration data were normalized to hLEC control group [*upper graph* in (**C**)] and to the siDS control group for siRNA experiments [*lower graph* in (C)]. $^*p < 0.05$, $^{\#}p < 0.01$, as compared to hLEC control group in (B) and (C) *upper graphs*, and to siDS control group in (B) and (C) *lower graphs*.

filters, and fluorescence-labeled BMDCs were loaded on top of the insert. Invading BMDCs into the collagen gel were quantified under various conditions that alter or inhibit HS produced by hLECs (Fig. 4A, 4B). The presence of normal hLECs in the collagen was able to drive invasion by DCs >200-fold over basal invasion into hLEC-free collagen. If invasion proceeded in the presence of blocking Ab to either CCR7 or its cognate ligands CCL19 and CCL21, invasion was significantly reduced, suggesting that CCR7-mediated signaling (in addition to the presence of the cognate CCR7 chemokine ligands) plays an important role in the invasion of DCs toward hLECs across collagen. The production of HS by hLECs was required for DC invasion, as initially evidenced by marked inhibition in the setting of heparinase-treated hLECs. Targeting the HS chain-initiating enzyme XylT2 or the sulfating enzyme Ndst1 also led to significant reductions in DC invasion. In contrast, Ab blockade of CCL5 or treatment with siRNA targeting Hs3st1 did not lead to significant reduction in DC invasion. These findings suggest distinct and specific requirements with respect to chemokines as well as the fine structure of lymphatic HS in the system.

Because LEC-derived HS may either be associated with core proteins (e.g., syndencans or glypicans) on the lymphatic cell surface or secreted into the extracellular space (e.g., perlecans), we further investigated whether targeting HS secreted by LECs might alter the ability of DCs to migrate, with the idea that LEC-secreted HS might play a *trans*-acting role in DC migration. Specifically, fluorescence-labeled BMDCs on transwell filters were separated from the HS-targeted hLEC monolayer in lower wells by liquid medium, and DC migration into lower wells was quantified (5). The presence of hLECs in the bottom well was sufficient to drive DC migration (Fig. 4C, 4D), and destroying HS with heparinase, blocking CCR7/CCL21 (Fig. 4C) and CXCR4/CXCL12 (Fig. 4D), or interfering with the biosynthesis of hLEC HS (Fig. 4E, using siRNA targeting Ndst1 and XylT2) significantly reduced DC migration. In contrast, CCL5-blocking Ab, CCL19-blocking Ab, or treatment of hLECs with Hs3st1 siRNA was not sufficient to alter migration (Fig. 4C–E). This suggests that the presence as well as specific sulfation properties (i.e., *N*-sulfation but not 3-*O*-sulfation) of HS produced into the hLEC-CM is critical for mediating CCL21- and CXCL12-dependent migration of DCs toward the hLECs. Furthermore, when we combined targeting approaches, that is, heparinase treatment of the hLECs together with blocking Abs to CCR7 or CCL21, we detected no further reduction in BMDC chemotaxis as compared to that noted for each individual treatment alone (Fig. 4F), suggesting that the CCL21/CCR7-mediated effects under these conditions appear to fully depend on lymphatic endothelial HS.

HS secreted from LECs is required for optimal binding of chemokines to cognate receptors on DCs

The finding that the migration of BMDCs is sensitive to altering HS produced by hLECs across liquid medium prompted us to explore the molecular mechanisms by which HS secreted by hLECs modulate DC migration. Given that CCR7/CCL21 and CCR4/CXCL12 signaling is essential for DC migration (Fig. 4C, 4D), and that HS is known to interact with basic amino acid motifs on several chemokines, including CCL21 and CXCL12 (8), we focused on the chemokine–receptor binding that might be affected by altering HS secreted by hLECs. For this purpose, CM was harvested from either control siRNA (siDS)–transfected hLECs or an equal number of hLECs transfected with siNdst1 or siXylT2 and applied to BMDCs. The interaction between CCL21 in the CM and CCR7 expressed on BMDCs was measured using the PLA, wherein a fluorescent signal will be generated when and only when the two target proteins are in close proximity (i.e., when the chemokine binds to its cognate receptor). The engagement of numerous cell surface CCL21/CCR7 complexes was noted upon exposure of BMDCs to CM from control hLECs (Fig. 5A, CM-siDS). Significant reduction in CCL21/CCR7 complexes was noted upon the application of CM from siNdst1-targeted hLECs (CM-siNdst1), and further reduction occurred upon exposing BMDCs to siXylT2-targeted CM (CM-siXylT2; Fig. 5A, 5B). Similar (albeit somewhat less dramatic) effects were also observed for the interaction between CXCL12 and CXCR4 on BMDCs

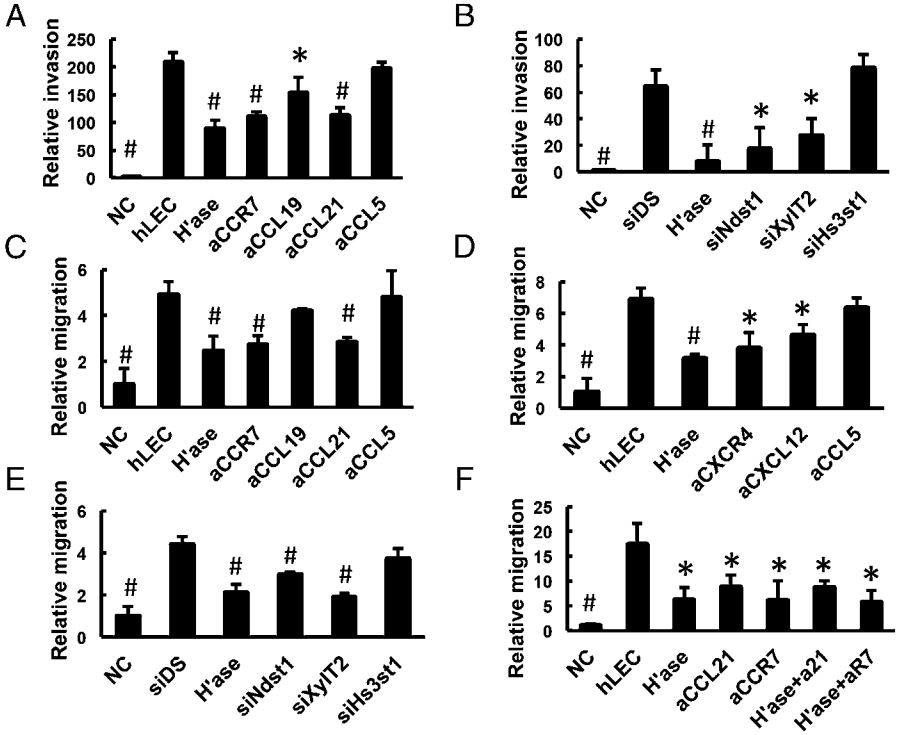

FIGURE 4. Invasion and migration of BMDCs depends on lymphatic HS. (**A** and **B**) Invasion of BMDCs at day 9 of differentiation into a collagen gel containing either no cells (NC) or hLECs treated as indicated was quantified and normalized to NC. (**C**–**F**) Transwell migration of BMDCs into wells containing NC or hLEC monolayer treated as indicated was quantified and normalized to NC. Anti-CCR7 [also aR7 in (F)], anti-CCL19, anti-CCL21 [also a21 in (F)], anti-CXCR4, anti-CXCL12, or anti-CCL5 indicates blocking Abs to CCR7, CCL19, CCL21, CXCR4, CXCL12, or CCL5, respectively; H'ase, hLECs pretreated with heparinase; siDS, hLECs transfected with control siRNA; siNdst1, siXylT2, or siHs3st1, hLECs transfected with siRNA targeting corresponding HS biosynthetic enzymes. $^{*}p < 0.05$, $^{\#}p < 0.01$, as compared to hLEC control group in (A), (C), (D), and (F), and to siDS control group in (B) and (E).

(Fig. 5C, 5D). Vehicle medium, the basal medium used to collect CM from hLECs, produced minimal CCL21/CCR7 or CXCL12/CXCR4 complexes (Fig. 5A, 5C), implying that PLA signal depends on the presence of these chemokines in the CM. Given that transient transfection of hLECs with different siRNA did not dramatically change the expression of CCL21 (Supplemental Fig. 3B) or its secretion into CM (5), the PLA data suggest that the optimal binding of chemokine to receptor on the BMDC surface depends on the presence of intact lymphatic HS produced into the CM (where it essentially acts in *trans* as a co-receptor).

Lymphatic endothelial HS facilitates oligomerization of lymphatic chemokines

The diversity of chemokine oligomerization has been shown to initiate distinct signaling responses and is known to be stabilized by HS glycosaminoglycans (17). To understand whether targeting lymphatic endothelial HS leads to alterations in chemokine oligomerization, we purified HS from confluent monolayers of hLECs transfected with either siDS, siXylT2, siNdst1, or siHs3st1 and incubated two different doses of the various purified siRNA-targeted HS species with recombinant human CCL21 (molecular mass, 12.2 kDa). We then examined the pattern of CCL21 oligomerization following crosslinking and gel electrophoretic separation of multimeric products. As shown in Fig. 6A, at the lower dose tested, HS from siDS- or siHs3st1-transfected hLECs led to robust CCL21 oligomerization, with distinct bands separated by approximately the size of a CCL21 monomer and the highest detectable oligomer being what appears to be an octamer (and a smear-like extension toward possibly larger products). In contrast, the same dose of HS from siXylT2- or siNdst1-transfected hLECs could only facilitate the formation of CCL21 trimers and tetramers, respectively. In the latter case, even at the higher HS dose, the purified siNdst1-altered HS could not support the formation of CCL21 oligomers greater than tetramer size (Fig. 6A), suggesting that targeting lymphatic endothelial HS biosynthesis at the level of initial chain formation or *N*-sulfation, but not 3-*O*-sulfation, dramatically reduces its capability to support the complexing of larger chemokine oligomers in this assay. A similar HS effect on CXCL12 (molecular mass, 8 kDa) oligomerization was also observed (Fig. 6B), with HS isolated from mock-transfected (siDS) control cells, but not from siXylT2 or siNdst1-transfected cells, strongly supporting CXCL12 multimerization.

Discussion

In this study, we provide genetic evidence that targeting the *N*-sulfation of lymphatic endothelial HS significantly reduces in vivo DC trafficking from the periphery to the draining LN, with the functional consequence of inhibiting $CD8^+$ T cell proliferation in the draining LN in response to OVA immunization. Mechanistically, lymphatic endothelial HS may mediate DC trafficking at multiple steps, including adhesion to LECs under flow as well as chemokine-dependent migration toward lymphatic endothelium. Moreover, appropriately sulfated lymphatic HS appears to be required for chemokine oligomerization and optimal presentation of certain chemokines such as CCL21 and CXCL12 on the DC surface.

The development of effective approaches to manipulate DC traffic has been limited by a lack of understanding of the molecular controls for this process. A few studies, including our own, have demonstrated that altering vascular HS biosynthesis, either through an alteration in *N*-sulfation of nascent HS chains (*Ndst1* mutation) or chain polymerization (*Ext1* mutation), results in altered chemokine-dependent interactions of endothelial cells with trafficking neutrophils, DCs, and tumor cells as they home to sites of

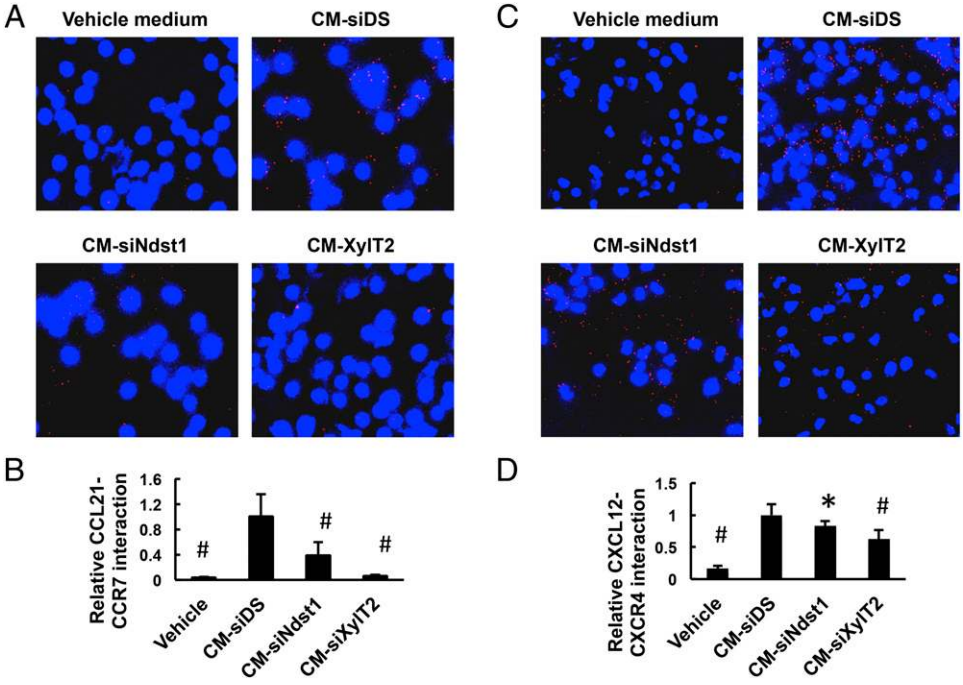

FIGURE 5. Presence of appropriately sulfated HS in lymphatic endothelial CM is required for binding of CCL21 to BMDCs. CM was collected from hLECs transfected with either siDS or siRNA targeting the HS biosynthetic enzymes Ndst1 or XylT2. Cytospin samples of day 9 BMDCs were incubated with the different CM. Binding of CCL21 in the CM to CCR7 on BMDCs was detected by PLA. (**A** and **C**) Representative merged images showing PLA signal (red) and nuclear DAPI stain (blue) were taken by fluorescence microscopy (original magnification, ×400). Signal for BMDCs incubated in the vehicle CM alone (EBM2 containing 5% horse serum, which served as the basal medium for all hLEC CM) is shown in the *upper left panel*. (**B** and **D**) PLA signal from each field was quantified and indexed to total nuclear area within the same field. The average of at least five random fields from each group was included for analysis, with mean data normalized to control signal (CM-siDS) (see graph below). $^*p < 0.05$, $^\#p < 0.01$, as compared to CM-siDS group.

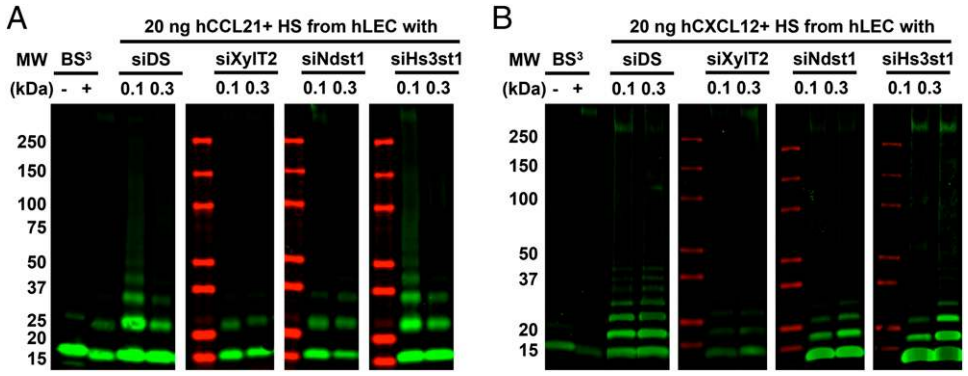

FIGURE 6. Lymphatic endothelial HS is essential for optimal oligomerization of CCL21 and CXCL12. HS was purified from cultured hLEC monolayers (grown in 10-cm plates) that were transfected with either siDS or siRNA targeting the indicated HS biosynthetic enzymes, and resuspended in 500 μl PBS. Recombinant human CCL21 [hCCL21, 20 ng/reaction, molecular mass, 12.2 kDa (**A**)] or hCXCL12 [20 ng/reaction, molecular mass, 8 kDa (**B**)] was incubated with 0.1 μl and 0.3 μl of each HS prep, followed by BS^3-mediated crosslinking, and separation on SDS-PAGE gels with detection by Western immunoblotting. Green signal, hCCL21 (A) or hCXCL12 (B) as detected by Western immunoblot; red signal, protein size marker. – and +, pure hCCL21 or hCXCL12 in the absence or presence of BS^3 crosslinker, respectively.

inflammation or colonize lymphoid organs via blood vascular or lymphatic vascular routes (5, 6, 18). For example, a panendothelial mutation in *Ext1* inhibits CCL21/CCL19 binding to LECs and impairs DC migration to the draining LN (6). Although this suggests what may occur when HS chains are absent or enzymatically ablated in the entire circulation, the degree to which lymphatic endothelial-specific alteration in HS affects DC traffic and specific T cell responses to Ag has not been reported. We stringently interrogated the role of lymphatic vascular-specific HS, separate from any role that blood endothelial HS might play in affecting T cell traffic through the blood vasculature (such as LN high endothelial venules). Moreover, HS is endowed with functional specificity for distinct ligands such as chemokines that may variably bind as a result of specific sulfate modifications. Targeting of the latter has also not been explored in the lymphatic system.

We inducibly knocked down *Ndst1* in lymphatic vasculature and demonstrated impairments in DC traffic in models that allow examination of movement of endogenous DCs (utilizing FITC plus oxazolone skin painting) as well as the traffic of exogenously loaded BMDCs to regional LNs. Because pathologically stimulated lymphatic endothelium may potentially undergo impaired growth/remodeling responses in the setting of HS mutations (19), a control experiment confirmed that induction of lymphatic endothelial *Ndst1* knockdown in the skin under basal/nonstimulated conditions does not alter lymphatic vascular density (Fig. 1B). Moreover, no significant changes in the total DC number within the skin were noted upon *Ndst1* knockdown at baseline, suggesting that reduced DC colonization within the draining LN (Fig. 1A, 1D) is caused by the effect of lymphatic-specific HS mutation on the DC trafficking process itself. To what extent the mutation might result in a defect in slowing/arresting of DCs as they enter the interfollicular sinuses from afferent lymphatics entering the LN is unknown, although a sophisticated analysis of this may be worthwhile in future studies.

To test downstream DC-dependent immunologic events, we asked how targeting the *N*-sulfation of lymphatic HS would affect T cell responses in the draining LN upon Ag stimulation. In a sensitization-elicitation allergic reaction model employing OVA Ag, we observed significant reduction in the total $CD8^+$ T cell population within the draining LN (Fig. 2). Although this is a complex immune response that involves in vivo lymphatic DC trafficking at both sensitization and elicitation steps, the lack of an LN $CD8^+$ T cell response in lymphatic-HS mutants highlights the functional importance of appropriately sulfated lymphatic HS in modulating the magnitude of the DC-dependent LN immune response. Moreover, OVA contains multiple epitopes capable of activating distinct subtypes of T cells, including $CD8^+$ cytotoxic and $CD4^+$ helper T cells (20), potentially mediated by DCs of different subsets or at distinct maturation or activation stages. With this in mind, the specific reduction of a $CD8^+$ T cell proliferative response but not that of the $CD4^+$ T cells reveals the unique effect of silencing lymphatic HS on the LN balance of T cell responses. As a final control, we "dissected" the importance of lymphatic-specific HS from that of blood-vascular HS in this immunization process by repeating the experiment in $Ndst1^{f/f}TekCre^+$ mutant mice (with a panendothelial deficiency in HS sulfation). A nearly identical result in terms of the $CD8^+$ T cell phenotype in the LN was observed, highlighting the importance of lymphatic-specific HS in the immune phenotype.

The molecular diversity of HS is highlighted by the ability of its unique sulfate-modified structural motifs to facilitate and/or mediate protein interactions that are essential for a variety of biological processes (14). However, knowledge is lacking with respect to how specific HS modifications contribute to mechanistic steps involved in functional immune responses. In cell-based assays, we found that by targeting the integrity of HS with heparinase or by blocking LEC biosynthesis of HS via siRNA, DC adhesion under flow and LEC-driven collagen invasion and matrix-independent migration were all significantly reduced. This was associated with chemokine specificity as well as HS fine-structure specificity in the system. Blockade was achieved using Abs to CCR7/CCL21 or CXCR4/CXCL12 but not CCL5, and the effects of silencing *N*-sulfation of LEC HS as opposed to 3-*O*-sulfation (siHs3st1) are consistent with data regarding the importance of *N*-sulfation and 2-*O*-sulfation (both of which result from Ndst1 silencing) (5, 18) as opposed to 3-*O*-sulfation for binding of CCL21 or CXCL12 to immobilized HS on glycan arrays (8). The trends in specificity suggest that chemokines that drive this system may work cooperatively with key sulfate motifs on HS produced by the LECs.

Other soluble regulators that might affect DC trafficking to the LN include selectin adhesion molecules, integrin family members, metalloproteinases, and possibly other chemokines (21–24). Importantly, we found that upon disruption of lymphatic HS biosynthesis in a low shear-rate flow model of DC over primary LECs, DC–LEC adhesion events were markedly inhibited. Alternatively, HS-mediated adhesion did not appear to be required for transmigration in this model, whereas Ab-mediated blocking

of CCR7/CCL21 had a significant impact on both DC–LEC adhesion as well as DC transmigration across hLECs under flow. The lack of HS effect on transmigration in this in vitro assay, as opposed to our in vivo findings supporting the role HS in orchestrating DC entry into lymphatic vessels by modulating CCL21 haptotaxis, may also be attributed to the fact that most adhesion events required for subsequent transmigration in some in vitro models may be less dependent on HS-mediated chemokine sequestration because the adherent DCs are in direct contact with the LEC monolayer under the force of gravity alone, which might be sufficient to engage the necessary "machinery" for diapedesis. In contrast, in vivo DCs may require greater assistance from sequestered chemokines to navigate efficiently through tissues and make such contacts.

We followed phenotypic characterizations with mechanistic studies suggesting that LEC HS may essentially regulate chemokine-dependent signaling by DCs in multiple ways depending on the context in which HS is presented. Recent work demonstrates that perilymphatic CCL21 gradients likely depend on HS in the extracellular matrix (5–7). However, the reduced in vitro DC migration observed upon disrupting HS prompted us to look specifically into the importance of HS secreted by LECs in the presentation of chemokine to the migrating DCs. Expression of CCL21 by LECs in these systems did not appear to be reduced by treating the LECs with heparinase or transient transfection of LECs with siNdst1 or siXylT2 (Supplemental Fig. 3B). Nevertheless, we noted that the ability of CM from siXylT2 or siNdst1 targeted LECs to support partnerships between CCL21 and CCR7 (or CXCL12 and CXCR4) on the DC surface was markedly reduced in comparison to that of CM from siRNA-control LECs (Fig. 5). These observations suggest that LEC HS plays a critical role in supporting in *trans* presentation of these lymphatic chemokines to their receptors. A mechanistic explanation and extension of these findings highlights the possibility that LEC HS (whether bound to secreted HS proteoglycans or released as free chains) may serve as a soluble co-receptor for lymphatic chemokines to optimally interact with their receptors on the surface of trafficking DCs. This is supported by the fact that genetic alterations in LEC HS biosynthesis resulted in marked alterations in the ability of CCL21 to oligomerize on purified soluble HS from mutant LECs as opposed to HS from wild-type/control LECs (Fig. 6).

The findings of this study contribute to our understanding of basic mechanisms that regulate DC migration and immunity. More generally, because DC traffic may become dysregulated in disorders such as autoimmunity, transplant rejection, or cancer, these findings suggest strategies for possibly reprogramming immunity through rational therapeutic interventions that modulate HS fine structure.

Acknowledgments

We acknowledge assistance from Dr Guillermo Oliver (St. Jude Children's Research Hospital) for provision of inducible *Prox1Cre* transgenic mutant mice as well as Dr. Jeffrey Esko (University of California San Diego) for provision of heparin lyases. We acknowledge Steven Kendall and Fluxion Biosciences for assistance with BioFlux plates and microfluidics system as well as Dr. Jennifer Meerloo of the University of California San Diego Microscopy Shared Facility. We thank Dr. Klaus Ley of the La Jolla Institute for Allergy and Immunology for assistance with analysis of DC subsets in the lymph node and Dr. Stephen Hedrick for provision of OT-I and OT-II transgenic mice. We also thank Dr. Phil Gordts for initial assistance with adoptive T cell transfers and Faye Nourollahi for additional assistance with mouse studies. We also acknowledge assistance and support from the Veterans Medical Research Foundation.

Disclosures

The authors have no financial conflicts of interest.

References

1. Förster, R., A. C. Davalos-Misslitz, and A. Rot. 2008. CCR7 and its ligands: balancing immunity and tolerance. *Nat. Rev. Immunol.* 8: 362–371.
2. Randolph, G. J., V. Angeli, and M. A. Swartz. 2005. Dendritic-cell trafficking to lymph nodes through lymphatic vessels. *Nat. Rev. Immunol.* 5: 617–628.
3. Delgado-Martín, C., C. Escribano, J. L. Pablos, L. Riol-Blanco, and J. L. Rodríguez-Fernández. 2011. Chemokine CXCL12 uses CXCR4 and a signaling core formed by bifunctional Akt, extracellular signal-regulated kinase (ERK)1/2, and mammalian target of rapamycin complex 1 (mTORC1) proteins to control chemotaxis and survival simultaneously in mature dendritic cells. *J. Biol. Chem.* 286: 37222–37236.
4. Capila, I., and R. J. Linhardt. 2002. Heparin-protein interactions. *Angew. Chem. Int. Ed. Engl.* 41: 391–412.
5. Yin, X., J. Truty, R. Lawrence, S. C. Johns, R. S. Srinivasan, T. M. Handel, and M. M. Fuster. 2010. A critical role for lymphatic endothelial heparan sulfate in lymph node metastasis. *Mol. Cancer* 9: 316.
6. Bao, X., E. A. Moseman, H. Saito, B. Petryniak, A. Thiriot, S. Hatakeyama, Y. Ito, H. Kawashima, Y. Yamaguchi, J. B. Lowe, et al. 2010. Endothelial heparan sulfate controls chemokine presentation in recruitment of lymphocytes and dendritic cells to lymph nodes. *Immunity* 33: 817–829.
7. Weber, M., R. Hauschild, J. Schwarz, C. Moussion, I. de Vries, D. F. Legler, S. A. Luther, T. Bollenbach, and M. Sixt. 2013. Interstitial dendritic cell guidance by haptotactic chemokine gradients. *Science* 339: 328–332.
8. de Paz, J. L., E. A. Moseman, C. Noti, L. Polito, U. H. von Andrian, and P. H. Seeberger. 2007. Profiling heparin-chemokine interactions using synthetic tools. *ACS Chem. Biol.* 2: 735–744.
9. Inaba, K., M. Inaba, N. Romani, H. Aya, M. Deguchi, S. Ikehara, S. Muramatsu, and R. M. Steinman. 1992. Generation of large numbers of dendritic cells from mouse bone marrow cultures supplemented with granulocyte/macrophage colony-stimulating factor. *J. Exp. Med.* 176: 1693–1702.
10. Quah, B. J., H. S. Warren, and C. R. Parish. 2007. Monitoring lymphocyte proliferation in vitro and in vivo with the intracellular fluorescent dye carboxyfluorescein diacetate succinimidyl ester. *Nat. Protoc.* 2: 2049–2056.
11. Yardeni, T., M. Eckhaus, H. D. Morris, M. Huizing, and S. Hoogstraten-Miller. 2011. Retro-orbital injections in mice. *Lab Anim. (NY)* 40: 155–160.
12. Livak, K. J., and T. D. Schmittgen. 2001. Analysis of relative gene expression data using real-time quantitative PCR and the $2^{-\Delta\Delta C(T)}$ method. *Methods* 25: 402–408.
13. Grobe, K., M. Inatani, S. R. Pallerla, J. Castagnola, Y. Yamaguchi, and J. D. Esko. 2005. Cerebral hypoplasia and craniofacial defects in mice lacking heparan sulfate *Ndst1* gene function. *Development* 132: 3777–3786.
14. Bishop, J. R., M. Schuksz, and J. D. Esko. 2007. Heparan sulphate proteoglycans fine-tune mammalian physiology. *Nature* 446: 1030–1037.
15. Lutz, M. B., N. Kukutsch, A. L. Ogilvie, S. Rössner, F. Koch, N. Romani, and G. Schuler. 1999. An advanced culture method for generating large quantities of highly pure dendritic cells from mouse bone marrow. *J. Immunol. Methods* 223: 77–92.
16. Desai, U. R., H. M. Wang, and R. J. Linhardt. 1993. Substrate specificity of the heparin lyases from *Flavobacterium heparinum*. *Arch. Biochem. Biophys.* 306: 461–468.
17. Salanga, C. L., and T. M. Handel. 2011. Chemokine oligomerization and interactions with receptors and glycosaminoglycans: the role of structural dynamics in function. *Exp. Cell Res.* 317: 590–601.
18. Ando, T., P. Jordan, T. Joh, Y. Wang, M. H. Jennings, J. Houghton, and J. S. Alexander. 2005. Isolation and characterization of a novel mouse lymphatic endothelial cell line: SV-LEC. *Lymphat. Res. Biol.* 3: 105–115.
19. Yin, X., S. C. Johns, R. Lawrence, D. Xu, K. Reddi, J. R. Bishop, J. A. Varner, and M. M. Fuster. 2011. Lymphatic endothelial heparan sulfate deficiency results in altered growth responses to vascular endothelial growth factor-C (VEGF-C). *J. Biol. Chem.* 286: 14952–14962.
20. Beacock-Sharp, H., A. M. Donachie, N. C. Robson, and A. M. Mowat. 2003. A role for dendritic cells in the priming of antigen-specific $CD4^+$ and $CD8^+$ T lymphocytes by immune-stimulating complexes in vivo. *Int. Immunol.* 15: 711–720.
21. Förster, R., A. Braun, and T. Worbs. 2012. Lymph node homing of T cells and dendritic cells via afferent lymphatics. *Trends Immunol.* 33: 271–280.
22. Johnson, L. A., and D. G. Jackson. 2010. Inflammation-induced secretion of CCL21 in lymphatic endothelium is a key regulator of integrin-mediated dendritic cell transmigration. *Int. Immunol.* 22: 839–849.
23. Rouzaut, A., S. Garasa, A. Teijeira, I. González, I. Martinez-Forero, N. Suarez, E. Larrea, C. Alfaro, A. Palazón, J. Dubrot, et al. 2010. Dendritic cells adhere to and transmigrate across lymphatic endothelium in response to IFN-α. *Eur. J. Immunol.* 40: 3054–3063.
24. Li, P., Z. J. Zhao, F. Y. Liu, L. Y. Sun, X. Ding, W. Z. Zhang, D. H. Shang, and C. F. Sun. 2010. The chemokine receptor 7 regulates cell adhesion and migration via β1 integrin in metastatic squamous cell carcinoma of the head and neck. *Oncol. Rep.* 24: 989–995.